The Iron Oxidation and Hydrolysis Chemistry of *Escherichia coli* Bacterioferritin†

Xiaoke Yang,‡ Nick E. Le Brun,§ Andrew J. Thomson,§ Geoffrey R. Moore,§ and N. Dennis Chasteen*,‡

Department of Chemistry, University of New Hampshire, Durham, New Hampshire 03824, and Center for Metalloprotein Spectroscopy and Biology, School of Chemical Sciences, University of East Anglia, Norwich NR4 7TJ, Great Britain

Received November 15, 1999; Revised Manuscript Received February 8, 2000

ABSTRACT: Bacterioferritins are members of a class of spherical shell-like iron storage proteins that catalyze the oxidation and hydrolysis of iron at specific sites inside the protein shell, resulting in formation of a mineral core of hydrated ferric oxide within the protein cavity. Electrode oximetry/pH stat was used to study iron oxidation and hydrolysis chemistry in *E. coli* bacterioferritin. Consistent with previous UV−visible absorbance measurements, three distinct kinetic phases were detected, and the stoichiometric equations corresponding to each have been determined. The rapid phase 1 reaction corresponds to pairwise binding of 2 Fe^{2+} ions at a dinuclear site, called the ferroxidase site, located within each of the 24 subunits, viz., $2Fe^{2+} + P^Z \rightarrow [Fe_2-P]^Z + 4H^+$, where P^Z is the apoprotein of net charge *Z* and $[Fe_2-P]^Z$ represents a diferrous ferroxidase complex. The slower phase 2 reaction corresponds to the oxidation of this complex by molecular oxygen according to the net equation: $[Fe_2-P]^Z + {}^1/_2O_2 \rightarrow [Fe_2O-P]^Z$ where $[Fe_2O-P]^Z$ represents an oxidized diferric ferroxidase complex, probably a μ-oxo-bridged species as suggested by UV−visible and EPR spectrometric titration data. The third phase corresponds to mineral core formation according to the net reaction: $4Fe^{2+} + O_2 + 6H_2O \rightarrow 4FeO(OH)_{(core)} + 8H^+$. Iron oxidation is inhibited by the presence of Zn^{2+} ions. The patterns of phase 2 and phase 3 inhibition are different, though inhibition of both phases is complete at 48 Zn^{2+}per 24mer, i.e., 2 Zn^{2+} per ferroxidase center.

The ferritins are a class of iron oxidation and mineralization proteins widely distributed among animals, microbes, and plants (*1*−*5*). Ferritins are composed of 24 similar or identical subunits assembled to form a hollow spherical structure with a central cavity of ∼80 Å diameter within which a hydrous iron(III) oxide mineral core is laid down. Oxidation and mineralization in the interior of the protein cavity is facilitated by the presence of protein ferroxidase and nucleation sites. These sites are important for rapid initial oxidation of iron(II) to iron(III) and its subsequent hydrolysis and mineralization on the inner surface of the protein (*3, 5*).

While the ferritins share many common features, there are significant differences between them. Mammalian ferritins are composed of two types of subunits, H and L, with approximately 54% homology in amino acid sequence between them (*5, 6*). The subunits have different functions: the H-subunit contains a ferroxidase center important for rapid Fe^{2+} oxidation while the L-subunit contains a cluster of acidic residues believed to be involved in mineral core nucleation (*6, 7*). In contrast, *Escherichia coli* bacterioferritin (EcBFR)[1] has a single type of subunit that contains both ferroxidase and nucleation sites (*2*−*4, 8, 9*). In addition, this protein contains up to 12 protoporphyrin IX heme groups of unknown function, buried within the protein shell between identical subunits related by 2-fold symmetry. The heme is axially coordinated to symmetry-related residues Met52 and Met52′ of the dimer of subunits (*9*−*12*). The ferroxidase centers of mammalian H-subunits and bacterioferritin subunits also differ significantly (Figure 1). Both iron atoms of EcBFR have histidine coordination and are bridged by two carboxylate residues (Glu51 and Glu127). In HuHF, only one iron has histidine coordination (His65), the other having Glu61 at the equivalent position, and the sites are bridged by only one carboxylate residue (Glu62). The effect of these differences is that one of the two sites at each center is almost identical (left site, Figure 1) while the other is very different (right site, Figure 1). Such differences in structure and subunit composition between mammalian ferritins and bacterioferritins may lead to differences in their iron oxidation and hydrolysis chemistry.

The iron oxidation/hydrolysis reactions for human and horse ferritins have recently been elucidated using electrode oximetry in conjunction with pH stat measurements (*13*−*15*). Iron binding, oxidation, and hydrolysis at the ferroxidase site of mammalian ferritins is described by eqs 1 and 2:

$$2Fe^{2+} + P^Z \rightarrow [Fe_2-P]^{Z+4} \quad (1)$$

$$[Fe_2-P]^{Z+4} + O_2 + 3H_2O \rightarrow [Fe_2O(OH)_2-P]^{Z+2} + H_2O_2 + 2H^+ \quad (2)$$

where P^Z is the apoprotein with a net charge *Z* and $[Fe_2-P]^{Z+4}$ and $[Fe_2O(OH)_2-P]^{Z+2}$ represent a dinuclear Fe^{2+} complex at the ferroxidase site and a hydrolyzed μ-oxo-

† Supported by Grant R37 GM20194 from the National Institute of General Medical Sciences (N.D.C.) and by a grant from the Wellcome Trust (G.R.M. and A.J.T.).

* To whom correspondence should be addressed.
‡ University of New Hampshire.
§ University of East Anglia.

[1] Abbreviations: HuHF, human H-chain ferritin; HoSF, horse spleen ferritin; EcBFR, *Escherichia coli* bacterioferritin; EPR, electron paramagnetic resonance; IPTG, isopropyl β-D-thiogalactopyranoside; Mes, 2-(*N*-morpholino)ethanesulfonic acid.

10.1021/bi992631f CCC: $19.00
Published on Web 03/29/2000

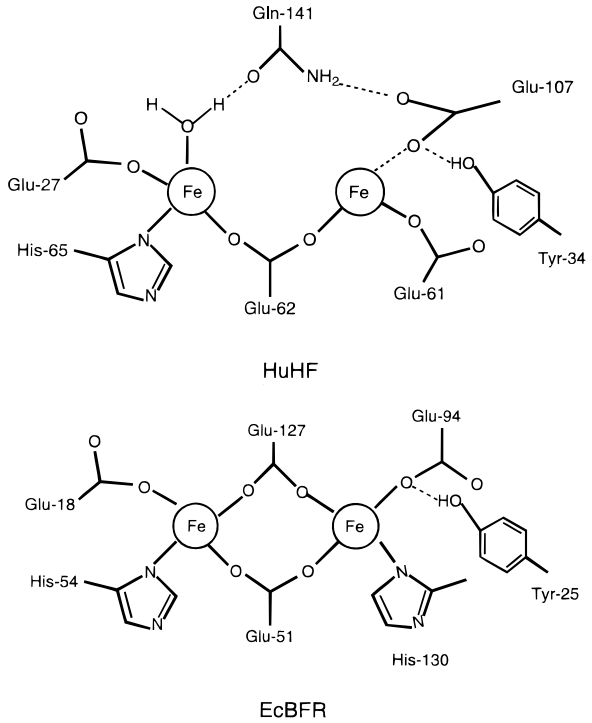

FIGURE 1: Schematic diagrams of the dinuclear ferroxidase sites of human H-chain ferritin and *Escherichia coli* bacterioferritin. The HuHF model is based on the crystal structure of the Tb^{3+} derivative (*5, 41*) and is probably most representative of the diferrous form; the diferric dimer probably contains one or more μ-oxo bridges (*13*). The EcBFR structure is based on the likely diMn(II) structure of Frolow et al. (*42*) and is a model for the diferrous form of the ferroxidase site.

bridged dinuclear iron(III) complex at the same site, respectively (*13*). In the ferroxidation reaction, H_2O_2 is produced from the two-electron reduction of dioxygen at the diiron site (*3, 5*). Recent studies with human and bullfrog ferritins indicate that a transient peroxo intermediate is formed in oxidation reaction 2 (*16, 17*).

The transfer of iron from the ferroxidase site to the mineral surface of mammalian ferritins occurs on a time scale of 5−10 min, regenerating the ferroxidase site for further oxidation of iron(II) (*13*). During iron migration from the ferroxidase site to the mineral core, further hydrolysis occurs according to eq 3. The net reaction for mineral core formation via the ferroxidase site is given by the sum of eqs 1, 2, and 3 (eq 4).

$$[Fe_2O(OH)_2{-}P]^{Z+2} + H_2O \rightarrow 2FeO(OH)_{(core)} + P^Z + 2H^+ \quad (3)$$

Net:

$$2Fe^{2+} + O_2 + 4H_2O \rightarrow 2FeO(OH)_{(core)} + H_2O_2 + 4H^+ \quad (4)$$

Once sufficient core has formed, the oxidation/hydrolysis reaction shifts to a mineral surface mechanism, becomes autocatalytic, and has the reaction stoichiometry given by eq 5. At the mineral surface, dioxygen undergoes an overall four-electron reduction to form water.

$$4Fe^{2+} + O_2 + 6H_2O \rightarrow 4FeO(OH)_{(core)} + 8H^+ \quad (5)$$

In the present study, we have examined the iron oxidation and hydrolysis chemistry of bacterioferritin from *E. coli* and find quite different behavior from that of the mammalian ferritins. Unexpectedly, the overall ferroxidase and mineralization reactions result in complete reduction of dioxygen to water. The slower mineralization reaction is not observed until iron in excess of 48 Fe^{2+}/apoprotein has been added, an amount necessary to saturate the 24 ferroxidase sites on the protein. In contrast to mammalian ferritins, the ferroxidase activity of EcBFR is not regenerated upon standing. However, iron oxidation at the ferroxidase site is necessary for the subsequent core formation reaction to occur at the wild-type rate. Addition of Zn(II) to the apoprotein prior to Fe^{2+} progressively inhibits the ferroxidase site reaction with complete inhibition at 48 Zn/protein. Zinc also inhibits the mineralization reaction but does so only after the first 24 Zn/protein have been added. The stoichiometric equations for the three kinetic phases of EcBFR are reported. The results are discussed in terms of possible mechanisms of core formation in bacterioferritin.

MATERIALS AND METHODS

Two EcBFR overexpression systems were used in the present work. One in which the *bfr* gene is expressed from its natural promoter (*8, 10*) was used to generate wild-type EcBFR and the site-directed variants M52H and E18A. The second involved the use of a derivative of pAlter-Ex1 (Promega), pGS758 (a kind gift from Dr. S. C. Andrews and Prof. J. R. Guest, University of Sheffield), in which the *bfr* gene is under control of an inducible *tac* promoter. This system, using *E. coli* JM109 as the host strain, was used to generate wild-type EcBFR. Expression of the *bfr* gene was induced by addition of IPTG (96 mg/L) when $A_{650\ nm}$ of the growing culture was ~0.15. For both systems, EcBFR was purified as previously described (*18*), except that for the pGS758 system, the final anion exchange chromatography step was omitted.

Protein concentration was determined using the bicinchoninic acid method with bovine serum albumin as a standard (*19*) or spectrophotometrically using an absorptivity of 33 000 cm^{-1} M^{-1} at 280 nm for the apoprotein. Heme concentration was determined using the pyridine hemochromogen method of Falk (*20*) and was found to be 5 and 1.3 for the wild-type EcBFR (first and second expression system, respectively) and 8.5 for variant E18A. Variant M52H did not contain any heme. Iron was removed from EcBFR by reduction with sodium dithionite and complexation with 2,2′-bipyridyl (*21*). Freshly prepared stock solutions of H_2O_2 were assayed by the amount of O_2 produced upon addition of the enzyme bovine catalase (Boehringer-Mannheim) as measured by Clark electrode oximetry.

Simultaneous measurements of O_2 uptake from Fe^{2+} oxidation and H^+ production from Fe^{2+} binding and Fe^{3+} hydrolysis were made using a specially designed 0.48 mL cell with sealable ports for delivery of standard base and reagents, and fitted with a Clark type oxygen, glass pH and Ag/AgCl reference microelectrodes. The cell was connected to a pH stat apparatus and an oxygen meter, both interfaced to a personal computer for collection of data in real time. The apparatus and methodologies employed in measuring rates of oxygen consumption and proton production and their

associated stoichiometries are described in detail elsewhere (*13*).

The half-lives for the response of the oxygen and pH electrodes are 2.3 and 0.8 s, respectively; thus, reaction rates with half-lives shorter than about 5 s cannot be accurately measured with the apparatus. To accurately measure initial rates of proton production, a pH stat proportional band setting of 0.2 had to be used; however, the rapid response of the pH stat at this setting lead to an overshoot of the stoichiometric end point at the end of the reaction. Therefore, the stoichiometry was determined in a separate experiment using a proportional band setting of 0.5 or 1.0 where the response of the pH stat was slower and an accurate end point could be obtained. Typical conditions for measurement were 2 μM protein in 50 mM NaCl, pH 6.5 (controlled by the pH stat), with increments of 12−48 Fe^{2+}/protein, added at 25 °C as freshly prepared 20.0 mM reagent-grade ferrous sulfate (Baker Scientific Inc.) in pH 3.4 water. Small corrections for free acid in the ferrous sulfate were made in all calculations. Zn^{2+} was added as 20.0 mM zinc(II) chloride (Sigma). Conditions for each experiment are given in the figure legends.

Quantitative EPR measurements were made at 77 K on a home-built spectrometer described elsewhere (*22*). The EPR signal intensity as a function of temperature over the range 10−100 K was determined with a Varian E-9 spectrometer fitted with a specially designed helium transfer cryostat (Cryo Industries). The concentration of Fe^{3+} responsible for the $g' = 4.3$ signal was determined from double integration of the $g' = 4.3$ region of the spectrum. A 0.27 mM diferric human serum transferrin sample was used as an EPR intensity standard as previously described for accurate spin concentration determinations on horse spleen ferritin (*23*).

The ultraviolet−visible difference spectrometric titration was performed on a Hewlett-Packard HP8453 single-beam diode array spectrometer. The instrument was zeroed using the 2 μM apoprotein solution as the blank. Spectra were repeatedly scanned until no further change in absorbance from Fe^{2+} oxidation was observed before the next increment of 20 mM ferrous sulfate was added to the sample. The time required between additions corresponded very well with the Fe^{2+} oxidation times observed by oximetry.

RESULTS

Previous spectrophotometric studies of the kinetics of EcBFR (30 °C, pH 6.5, 0.4−0.5 μM protein) indicated that core formation proceeds in three phases: a rapid first phase ($t_{1/2} \sim 50$ ms) corresponding to the binding of two Fe^{2+} to the ferroxidase site; a second slower phase ($t_{1/2} \sim 5$ s) in which the Fe^{2+}at the ferroxidase site is oxidized; and a third much slower phase ($t_{1/2} \sim 300$ s) that is seen only when more than 50 Fe are added to the protein (*24*). This latter phase corresponds to the mineralization of the iron core. In the present work, we examined the chemistry and kinetics of iron oxidation/hydrolysis at 25 °C for each of the three phases using the oximetry/pH stat apparatus.

The Phase 1 Reaction. To study the first phase corresponding to Fe^{2+} binding to the ferroxidase site without oxidation, 48 Fe^{2+} were added anaerobically to apo-EcBFR in 50 mM NaCl, and the production of protons was monitored by titration with standard base to maintain the pH. The data indicate that approximately two protons are generated per Fe^{2+} bound to the protein, i.e., 1.9 ± 0.1 H^+/Fe at pH 6.5. Similar proton counts have been observed for the binding of other divalent metal ions, e.g., Zn^{2+}, Mn^{2+}, and Co^{2+}, to the ferroxidase site of apo-EcBFR (*4, 25, 26*) and for Fe^{2+} binding to *Azotobacter vinelandii* bacterioferritin (*27*). Since the rate of proton production upon Fe^{2+} binding to apo-EcBFR for the phase 1 reaction exceeded the 0.8 s response time of the pH electrode, the rate of proton release could not be measured. We write the reaction for the first phase as

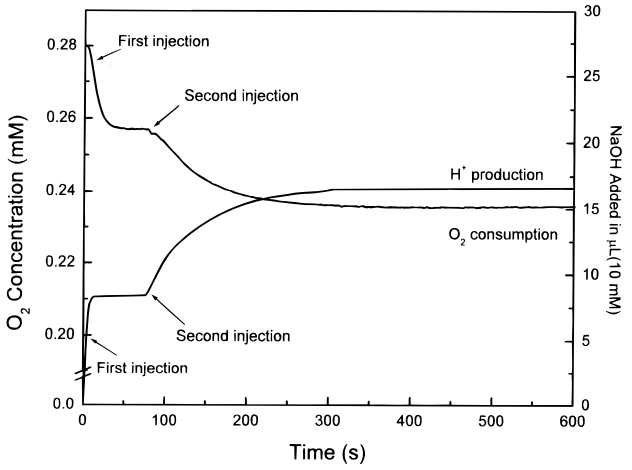

FIGURE 2: Oxygen consumption and proton production curves for injection of 48 Fe^{2+} per EcBFR followed by a second injection of 48 Fe^{2+}. Conditions: 2.0 μM protein, 50 mM NaCl, pH 6.5, 25 °C, with Fe^{2+} added as 20.0 mM $FeSO_4$.

$$2Fe^{2+} + P^Z \rightarrow [Fe_2{-}P]^Z + 4H^+ \quad (6)$$

where $[Fe_2{-}P]^Z$ represents the diferrous complex at the protein ferroxidase site.

The Phase 2 Reaction. To study the second phase, 48 Fe^{2+} were added aerobically to apo-EcBFR. In this experiment, both Fe^{2+} binding and its oxidation, i.e., phases 1 and 2, are measured. Both the uptake of O_2 and the production of H^+ were monitored as shown in Figure 2 (first injection). The rate of proton production is very rapid, exceeding the ability of the electrode to follow the kinetics, and is much faster than the rate of O_2 consumption. Even though the rate of proton production could not be reliably measured, the total amount of H^+ liberated could be accurately determined, giving an H^+/Fe stoichiometry of 2.2 ± 0.2, which is essentially the same as that for the phase 1 measurement noted above. We conclude that proton production arises solely from the rapid binding of Fe^{2+} to the protein during phase 1 and that essentially no protons are produced in the slower Fe^{2+} oxidation reaction of phase 2. From the total amount of O_2 consumed (Figure 2, first injection), we obtain a value of 4.1 ± 0.2 for the Fe^{2+}/O_2 stoichiometry and thus write the reaction for phase 2 as

$$[Fe_2{-}P]^Z + {}^1/_2O_2 \rightarrow [Fe_2O{-}P]^Z \quad (7)$$

where $[Fe_2O{-}P]^Z$ represents an oxidized diferric ferroxidase complex, probably a μ-oxo-bridged species (vide infra). Since the data provide no information as to the extent of

hydration of the dinuclear center, the reaction can alternatively be written as

$$[Fe_2{-}P]^Z + {}^1/_2O_2 + H_2O \rightarrow [Fe_2(OH)_2{-}P]^Z \quad (8)$$

The phase 2 reaction is first-order in total iron concentration since the initial rates for 24 Fe^{2+}/protein and 36 Fe^{3+}/protein samples (not shown) are 2 and 3 times as fast, respectively, as that of a 12 Fe^{2+}/protein sample at the same protein concentration. First-order dependence on iron is also illustrated by the observation that the initial rates of the phase 2 reaction for samples containing 12, 24, or 48 Fe^{2+}/protein are the same when divided by the Fe^{2+}concentration regardless of the protein concentration (Figure 3 caption). These observations also suggest that the rate depends only on the concentration of Fe^{2+} bound at the ferroxidase centers for experiments conducted at Fe^{2+}/protein ratios $\leq$48 and not on the protein concentration per se.

If the sample is allowed to stand for 10 min after the first addition of 48 Fe^{2+} prior to the addition of more iron, the phase 2 ferroxidase reaction is not regenerated nor is it regenerated when the experiment is performed at pH 7 and 37 °C, conditions where ferroxidase activity is regained in mammalian ferritins (*13*). Only phase 3 kinetics are observed. This finding is in accord with previous kinetic studies of EcBFR showing that a 24 h period between iron additions at 30 °C does not regenerate the phase 2 reaction (*24*).

The Phase 3 Reaction. To measure the third phase, 48 Fe^{2+} were added to the protein after the reaction of the initial 48 Fe^{2+} was complete (Figure 2, second injection). The initial rate of oxygen consumption in the third phase is markedly slower than that of the second phase, $t_{1/2} \sim 45$ s vs 6.5 s (25 °C, 50 mM NaCl, pH 6.5, 2 μM protein). Moreover, in phase 3, the measured rates of O_2 consumption and H^+ production are the same, and thus oxidation and hydrolysis occur simultaneously or nearly so within the time resolution of the apparatus (Figure 2, second injection). Reaction stoichiometries of $Fe^{2+}/O_2 = 4.3 \pm 0.2$ and $H^+/Fe^{2+} = 2.0 \pm 0.2$ were obtained from the data. Accordingly, we write the reaction for the third phase as

$$4Fe^{2+} + O_2 + 6H_2O \rightarrow 4FeO(OH)_{(core)} + 8H^+ \quad (9)$$

which is the same as the mineral surface reaction 5 previously observed for mammalian ferritins (*13, 28*).

Figure 3 shows more clearly the dependence of the initial rate of reaction on the iron/protein ratio as well as the transition between the second and third phases. In the three experiments shown, Fe^{2+} was titrated into the protein in increments of either 12, 24, or 48 Fe/protein shell, and the initial rate of O_2 consumption was measured after each addition. In all three instances, the initial rate falls off dramatically beyond 48 Fe per protein where only the slower phase 3 reaction is observed.

pH Dependence. Figure 4 illustrates the dependence of the initial rate of the phase 2 and 3 reactions on pH. The phase 2 ferroxidase reaction is pH-independent whereas the mineralization reaction (phase 3) shows an approximate $\sim[OH]^{1/2}$ dependence on base over the pH range of 6.0−7.5. Contrary to the present finding, previous work had suggested that the phase 2 reaction depends on pH but was based on limited data (*10*).

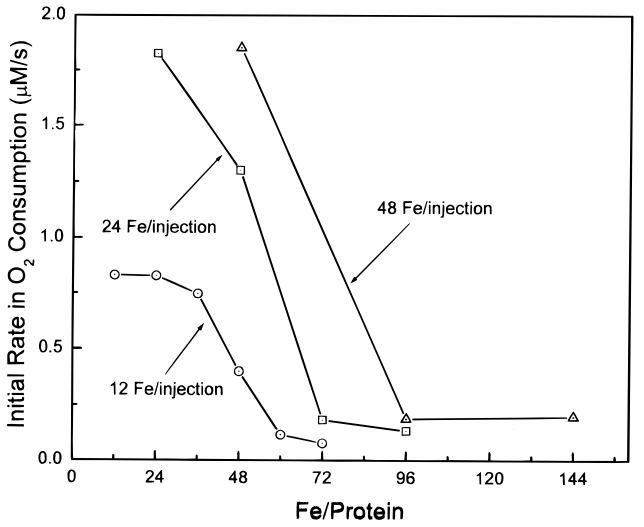

FIGURE 3: Dependence of the initial rate of oxygen consumption on the Fe^{2+}/EcBFR ratio. Additions were made in increments of 12, 24, or 48 Fe^{2+} per protein. Conditions: 4.0 μM protein for the 12 and 24 Fe^{2+} injections and 2.0 μM protein for the 48 Fe^{2+} injection, 50 mM NaCl, pH 6.5, 25 °C, with Fe^{2+} added as 20.0 mM $FeSO_4$. Initial rates per unit iron concentration (initial rate/$[Fe^{2+}]$) for the first injection of 12, 24, and 48 Fe^{2+} per protein are 0.017, 0.019, and 0.019 μM O_2/s·μM Fe, respectively.

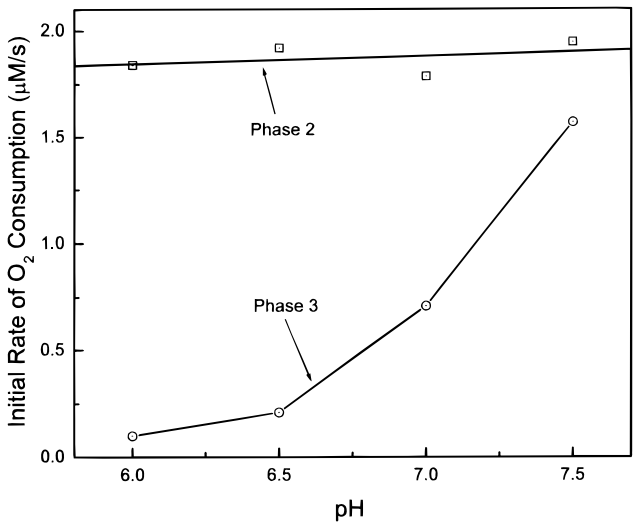

FIGURE 4: Dependence of the initial rate of the phase 2 and 3 reactions on pH. To measure the phase 2 kinetics, 48 Fe^{2+} were added to apo-EcBFR. To measure the phase 3 kinetics, a second addition of 48 $Fe^{2+}$was made. Conditions: 2.0 μM protein, 50 mM NaCl, 25 °C, with Fe^{2+} added as 20.0 mM $FeSO_4$.

Catalase Experiments. For both the phase 2 and phase 3 reactions, the addition of the enzyme catalase prior to the addition of iron to the protein had no effect on either the rate of iron oxidation or the measured Fe^{2+}/O_2 stoichiometry, a result consistent with the lack of production of measurable amounts of free H_2O_2 in solution. This finding contrasts with results for the mammalian ferritins where H_2O_2 is produced by the ferroxidase site reaction (eq 2) and catalase has an effect on the apparent stoichiometry of oxygen uptake (*13*−*15, 28*).

Neither the wild-type protein containing 5 heme groups nor the heme-free M52H variant (*10*), either as apoprotein or as protein containing 48 Fe, exhibited catalase activity when presented with hydrogen peroxide (50−80 μM), as

measured by the evolution of O_2. However, very low catalase activity was seen with the wild-type apoprotein and with a wild-type 48 Fe/protein preparation, both containing 1.3 hemes. This minimal activity for the 48 Fe/protein sample was about 1/300 of the ferroxidase activity of the protein and was completely inhibited by the addition of KCN. We ascribe this weak catalase activity to a likely contaminant in the preparation.

Reactivity toward Hydrogen Peroxide. To determine whether Fe^{2+} in EcBFR is preferentially oxidized by H_2O_2 (as opposed to O_2), 48 Fe^{2+} (96 μM) were added to a 2 μM protein sample containing both H_2O_2 (160 μM) and O_2 (280 μM), each oxidant being present in an amount sufficient to oxidize all of the iron. In a number of repeat experiments, only 25% of the O_2 was consumed relative to control experiments conducted in the absence of H_2O_2. Thus, H_2O_2 is a better oxidant of Fe^{2+} in the presence of EcBFR than is O_2. Similar results were obtained in the absence of protein, indicating that H_2O_2 is also a better oxidant than O_2 during simple autoxidation of Fe^{2+}. In contrast to the results with EcBFR, H_2O_2 produced at the ferroxidase site of mammalian ferritins accumulates in solution and is detected by O_2 generation in the presence of added catalase (*13*−*15*, *28*).

Zinc Inhibition. Zn^{2+} is a known inhibitor of iron oxidation in EcBFR (*29*). Accordingly, the effect of Zn^{2+} on the rates of the phase 2 and 3 reactions was examined. For the phase 2 reaction, the addition of varying amounts of Zn^{2+} to the apoprotein prior to the addition of 48 Fe^{2+} results in a linear decrease in the initial rate of oxygen consumption with added Zn^{2+} (Figure 5A); complete loss of ferroxidase activity is obtained at 48 Zn^{2+} added. To study the third phase, a second addition of 48 Fe^{2+} per protein was made. In contrast to the results for the ferroxidase reaction, the mineralization phase 3 reaction is not affected by the first 24 Zn^{2+} added; however, additional Zn^{2+} causes the rate of the mineralization reaction to likewise decline, ultimately being abolished at 48 Zn^{2+} added (Figure 5A). In a related experiment, varying amounts of Zn^{2+} were added first to the apo-EcBFR followed by an amount of Fe^{2+} to give a total amount of $Zn^{2+} + Fe^{2+}$ equal to 48. After the phase 2 kinetics were complete, 48 more Fe^{2+} were added and the phase 3 kinetics measured. Again, the phase 3 reaction was not inhibited until more than 24 Zn^{2+} were added to the protein and was completely abolished at 48 Zn^{2+} added (Figure 5B).

Variant M52H. Oximetry/pH stat measurements were also made on the EcBFR variant M52H which lacks heme (*10*). The same rates and stoichiometries were observed for the phase 2 and 3 reactions as for the heme containing wild-type protein (data not shown), a result indicating that the heme plays no role in the oxygen uptake kinetics. These findings are in accord with previous studies of iron oxidation conducted spectrophotometrically showing identical kinetics for the two proteins (*10*).

Variant E18A. The kinetics of iron oxidation/hydrolysis in the ferroxidase site variant E18A were also examined. In this variant, Glu18, a ligand of one of the irons of the dinuclear ferroxidase center (Figure 1), is changed to alanine (*29*). Despite the loss of the ligand Glu18, the variant is still able to facilitate iron oxidation, albeit at a rate one-sixth that of the wild-type protein. It also exhibits both phase 2 and phase 3 kinetics (Figure 6). Significantly, the changeover between the phase 2 and phase 3 kinetics occurs at 24 Fe^{2+} added to the protein, not 48 Fe^{2+}, suggesting that half of the dinuclear ferroxidase site remains functional, albeit with lower activity (Figure 6, inset). The overall reaction stoichiometries of the variant remain unchanged from those of the

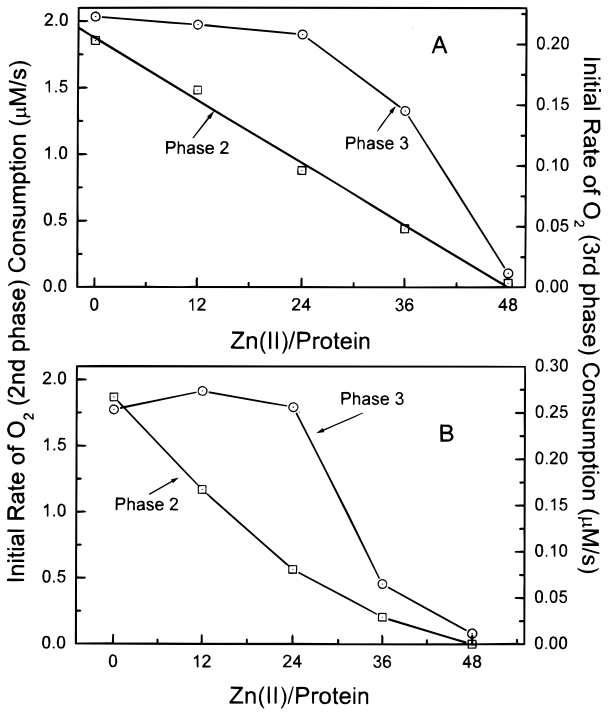

FIGURE 5: Inhibition of the initial rates of the phase 2 and 3 reactions by zinc(II). Panel A: Varying amounts of Zn^{2+} were added to apo-EcBFR and allowed to incubate for 5 min followed by the addition of 48 Fe^{2+} and the phase 2 kinetics measured. Then an additional 48 Fe^{2+} were added and the phase 3 kinetics measured. Panel B: The experiment was conducted in the same way as in panel A except that the first addition of Fe^{2+} varied such that the sum of the added Zn^{2+} plus Fe^{2+} was 48. Conditions: 4.0 μM protein, 50 mM NaCl, pH 6.5, 25 °C, with Fe^{2+} added as 20.0 mM $FeSO_4$ and Zn^{2+} added as 20.0 mM $ZnCl_2$. Each data point is for a different protein sample.

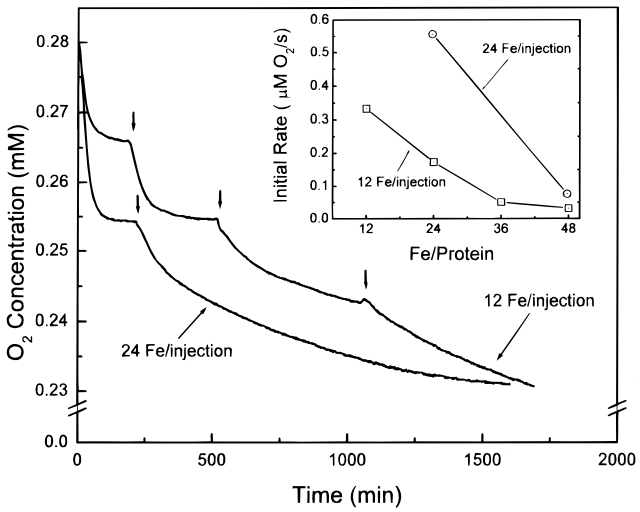

FIGURE 6: Oxygen consumption curves for variant E18A following 4 additions of 12 Fe^{2+} per protein and 2 additions of 24 Fe^{2+} per protein. Arrows denote times of additions. Inset: Dependence of the initial rate on the Fe^{2+}/protein ratio for the 12 and 24 Fe^{2+}/protein additions. Conditions: 4.0 μM protein, pH 6.5, 25 °C, with Fe^{2+} added as 20.0 mM $FeSO_4$.

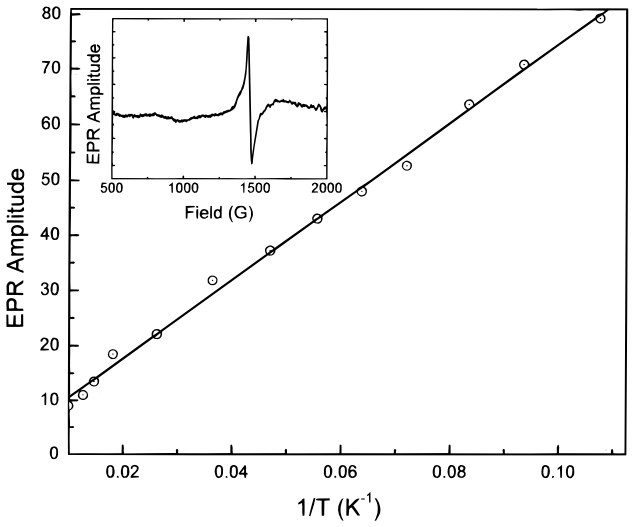

FIGURE 7: Curie plot of EPR signal intensity versus reciprocal temperature. Inset: EPR spectrum at 9.3 K. Conditions: 2 μM EcBFR, 24 Fe/protein, 50 mM NaCl, pH 6.5. Instrument parameters: scan range = 2000 G; scan time = 8 min; microwave frequency = 9.4 GHz; microwave power = 10 mW; modulation amplitude = 10 G; time constant = 1 s; receiver gain = 10^5; temperature range = 9.3−100 K.

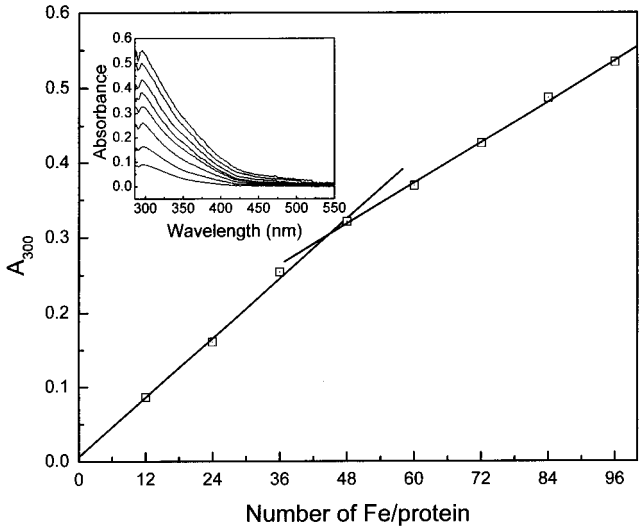

FIGURE 8: Spectrometric titration of apoEcBFR with ferrous sulfate. Inset: Family of UV−visible difference spectra. Conditions: 2 μM protein, 50 mM Mes, pH 6.5. The protein was titrated with 20 mM $FeSO_4$. See Materials and Methods for experimental details.

wild-type protein, namely, $Fe^{2+}/O_2 = 4$ and $H^+/Fe^{2+} = 2$, and they are the same stoichiometries as autoxidation.

Spectroscopic Measurements. Previous EPR studies of EcBFR following Fe^{2+} oxidation revealed the presence of a $g' = 4.3$ signal ascribed to a high-spin mononuclear Fe^{3+} species in an environment of low symmetry (*24*, *30*, *31*). To determine whether this species is the primary product of the phase 2 reaction, Fe^{2+} (24 or 48 Fe/protein) was added to the 2 μM apoprotein sample in the oximetry cell (pH stat = 6.5). After the phase 2 reaction was complete, the sample was immediately withdrawn and quickly frozen in an EPR tube, the total time elapsed being approximately 3 min. The characteristic $g' = 4.3$ EPR signal was observed (Figure 7, inset). The signal was undiminished upon thawing the sample for 30 min and refreezing it. The temperature dependence of the signal over the range 10−100 K followed the Curie law (Figure 7) which allows the concentration of iron(III) responsible for the signal to be determined without knowing the zero-field splitting parameter *D*. (*D* must be less than 2 cm^{-1} in EcBFR for Curie behavior to extend to 10 K.) When the $g' = 4.3$ signal was compared with that of diferric transferrin as an intensity standard, only 18% of iron in the 24 Fe/protein and 3% of the iron in the 48 Fe/protein were found to be EPR-active, indicating relatively little monomeric iron in these samples. Because of its isotropic character, the $g' = 4.3$ signal can be deceptively strong (Figure 7, inset) for the small amount of iron(III) it actually represents. The 24 Fe/protein sample was repeatedly thawed and refrozen over a period of 30 min. The signal intensity did not diminish. We conclude from these experiments that the monomeric Fe^{3+} complex is most likely not a major product of the ferroxidase reaction nor does it appear to be a transient species in the reaction since the $g' = 4.3$ signal, once formed, is relatively stable during the time scale of our experiments.

Ultraviolet−visible spectroscopy was therefore employed to study the product of the phase 2 reaction as done previously for horse spleen and human H-chain ferritins (*13*). A spectrometric titration of EcBFR with Fe^{2+} is shown in Figure 8 with the family of UV−visible difference spectra given in the inset. A discontinuity in 300 nm absorbance is evident at 48 Fe/protein, consistent with diferric dimers forming at each of the 24 ferroxidase centers of the protein. The molar absorptivities for the ferroxidase center iron and mineralized iron are 3380 M^{-1} cm^{-1} and 2030 M^{-1} cm^{-1} per iron, respectively. Similar spectrometric titrations have been reported for human H-chain and horse spleen ferritins with molar absorptivities of 2990 and 3540 M^{-1} cm^{-1}, and 2140 and 2285 M^{-1} cm^{-1} per iron for the ferroxidase center iron and mineralized iron of these proteins, respectively (*13*),[2] and are comparable to the values seen here for EcBFR. For mammalian ferritins, the band maximum at 300−310 nm has been attributed to an oxoligand to Fe^{3+} charge-transfer band of μ-oxo-bridged species (*13*). The assignment is based on data from model compounds and other dinuclear Fe^{3+} proteins and Mössbauer spectra showing μ-oxo-bridged dimer formation at the ferroxidase sites of the mammalian proteins (*13*, *21*, *32*). The results in Figure 8 suggest μ-oxo bridge formation in EcBFR as well, a proposal consistent with results of a preliminary Mössbauer study of EcBFR (*33*); however, further spectroscopic studies are needed to firmly establish the structural characteristics of the diferric dimer of the bacterial protein.

DISCUSSION

The experiments reported here provide new insights into the chemistry of iron oxidation and core mineralization in the ferritins. It is evident that the dinuclear iron center of the ferroxidase site plays a central role in the chemistry of the phase 1 and 2 reactions. That the chemistry examined in the present work takes place at the 24 dinuclear ferroxidase sites of EcBFR is evidenced by the stoichiometry of 48 Fe/protein for the phase 2 reaction (Figures 3 and 8), the complete inhibition of iron(II) oxidation upon addition of

[2] The previously reported molar absorptivities for HuHF and HoSF are on a per iron dimer basis (*13*). The values in ref *13* should be divided by 2 to obtain the correct values on a per iron basis.

48 Zn^{2+}/protein (Figure 5), and the greatly reduced rate of iron oxidation in the ferroxidase site variant E18A in which half of the ferroxidase site is presumably disabled, leading to an Fe/protein stoichiometry of 24/1 for the phase 2 reaction.

The dinuclear centers of the iron-mineralizing ferritins (Figure 1) have structures similar to those of the oxygen-activating enzymes ribonucleotide reductase and methane monooxygenase, the oxygen transport protein hemerythrin, and rubrerythrin, a protein of uncertain function (*2, 5*). The iron centers of all these proteins react with O_2 but process it in different ways. Within the ferritin family of proteins, the marked differences in the iron oxidation and hydrolysis chemistry between mammalian ferritins and bacterioferritins (cf. eqs 1−5 vs eqs 6−9) undoubtedly reside in differences in the structures of their dinuclear centers (Figure 1) and in the surrounding protein architecture. There are several major differences between the iron oxidation/hydrolysis chemistry of mammalian ferritins and bacterioferritins made evident from the present work: (1) In mammalian ferritins, only 0.2−0.3 H^+ is released per Fe^{2+} bound in the phase 1 reaction (*13*) compared to 2 H^+ per Fe^{2+} bound for EcBFR (this work). (2) The ferroxidase activity of mammalian ferritin is regenerated upon standing (*13, 15*) but is not in bacterioferritin (this work, *24*). (3) The mammalian ferritins show a bell-shaped pH dependence in the phase 2 reaction typical of an enzyme (*14, 15*) whereas in EcBFR the reaction is pH-independent. (4) Hydrogen peroxide is produced in the ferroxidase reaction of mammalian ferritin (*15, 28*) whereas water is produced in EcBFR.

Given that Fe^{2+} and its complexes do not readily hydrolyze at the pH values employed here (*34*), one assumes that the two protons liberated per Fe^{2+} bound to apo-EcBFR are derived from the protein ligands, namely, from the two histidine residues, His54 and His130, and two of the four glutamate residues, as previously proposed for the binding of other divalent metals to the protein (*25*). The charge balance achieved from the release of two protons upon binding of Fe^{2+} may account in part for the stability of the iron−protein complex and the failure of EcBFR to regenerate ferroxidase activity upon standing.

The observation of the same initial rate of oxidation per unit iron concentration for Fe^{2+}/protein ratios of 12, 24, and 48 (Figure 3 caption) suggests iron binding to the ferroxidase center occurs pairwise with relatively few singly occupied ferroxidase centers being present. This tentative conclusion is predicated on the assumption that the doubly iron occupied ferroxidase centers have greater ferroxidase activity than the singly occupied centers. The observed linear decrease in the phase 2 rate with added Zn^{2+}, up to 48 Zn^{2+} (Figure 5A), also suggests that Zn^{2+} binds pairwise to the ferroxidase center. Previous binding studies have shown that two Co^{2+} ions bind cooperatively to each ferroxidase center of EcBFR (*26*), a result in accord with the present kinetic data.

The lack of pH dependence in the phase 2 reaction of EcBFR (Figure 4) indicates that the forward reaction 6 is complete before reaction 7 takes place and that the reverse of reaction 6 has not yet occurred. If a preequilibrium (reversibility) were achieved for reaction 6 prior to reaction 7, an inverse dependence on $[H^+]^4$ would be expected for the phase 2 reaction,[3] contrary to what is observed (Figure 4). Furthermore, the phase 2 reaction is first-order in iron concentration (Results), not second-order as anticipated if eq 6 were an equilibrium reaction. In addition, the rate of the phase 2 reaction is independent of the protein concentration provided that the Fe^{2+}/protein ratio is less than 48, i.e., there are a sufficient number of protein ferroxidase sites to complex all of the iron (Figure 3 caption). It is only the concentration of the preformed $[Fe_2-P]^Z$ species (which is proportional to the iron concentration) that governs the phase 2 rate (eq 7) and not the forward reaction leading to $[Fe_2-P]^Z$ formation (eq 6), which is complete within ~50 ms (*24*). Thus, we conclude that the measured phase 2 kinetics reflect only the chemistry occurring in eq 7 as written.

Two general kinds of ferroxidation mechanism can be envisaged to explain the complete reduction of O_2 to water: one utilizes the Fe^{4+} oxidation state in a fashion similar to the dinuclear iron centers of ribonucleotide reductase and methane monooxygenase (*35, 36*), and the other involves O_2 reduction at one ferroxidase center to produce H_2O_2 followed by its rapid reduction to water at a second ferroxidase center. While the latter mechanism involving H_2O_2 production is consistent with our observation that H_2O_2 appears to be a better oxidant than O_2 for iron in BFR (Results), the participation of the ferroxidase centers of the protein in this process has not been demonstrated here. On the other hand, a picture is beginning to emerge as to how the dinuclear iron centers of animal ferritins produce H_2O_2 during iron oxidation whereas those of the enzymes ribonucleotide reductase and methane monooxygenase completely reduce O_2 during their Fe^{4+} catalytic cycles (*37*). Since water is produced in bacterioferritin and its dinuclear center more closely resembles those of the enzymes than does animal ferritin (*2, 5*), we initially focus our discussion on a possible mechanism of iron oxidation in BFR involving high-valent iron.

In the first step (eq 10) of the postulated mechanism, O_2 reacts with the $diFe^{2+}$ center to produce a peroxo diferric intermediate, $[Fe^{3+}(O_2^{2-})Fe^{3+}]-P$, which then decays to a $diFe^{4+}$ μ-oxo-bridged intermediate, $[Fe^{4+}(O^{2-})(O^{2-})Fe^{4+}]-P$:

$$[Fe^{2+}Fe^{2+}]-P + O_2 \rightarrow [Fe^{3+}(O_2^{2-})Fe^{3+}]-P \rightarrow [Fe^{4+}(O^{2-})(O^{2-})Fe^{4+}]-P \quad (10)$$

The high-valent intermediate then undergoes a redox-coupled reaction with another $diFe^{2+}$ ferroxidase center via the pair of reactions 11 and 12 to form 2 mol of μ-oxo-bridged $[Fe^{3+}(O^{2-})Fe^{3+}]-P$ dimer.

$$[Fe^{4+}(O^{2-})(O^{2-})Fe^{4+}]-P + 2H^+ + 2e^- \rightarrow [Fe^{3+}(O^{2-})Fe^{3+}]-P + H_2O \quad (11)$$

$$[Fe^{2+}Fe^{2+}]-P + H_2O \rightarrow [Fe^{3+}(O^{2-})Fe^{3+}]-P + 2H^+ + 2e^- \quad (12)$$

The net reaction, which is the sum of eqs 10−12, is given by eq 13 and has the same stoichiometry

[3] A steady-state treatment of the concentration of $[Fe_2-P]^Z$ does not apply here since reaction 6 is fast relative to reaction 7.

$$2[Fe^{2+}Fe^{2+}]-P + O_2 \rightarrow 2[Fe^{3+}(O^{2-})Fe^{3+}]-P \quad (13)$$

as the experimentally determined phase 2 reaction (eq 7). The reaction stoichiometry of eq 7 is also predicted by the two-step mechanism involving H_2O_2 production and consumption at successive ferroxidase centers. That mechanism is illustrated by eqs 14 and 15:

$$[Fe_2-P]^Z + O_2 + H_2O \rightarrow [Fe_2O-P]^Z + H_2O_2 \quad (14)$$

$$[Fe_2-P]^Z + H_2O_2 \rightarrow [Fe_2O-P]^Z + H_2O \quad (15)$$

Our present data do no enable us to distinguish between these two possible mechanisms.

There is no change in the net charge of the iron−protein complex during the phase 2 iron(II) oxidation step since no protons are involved in the reaction (eq 7 or 8). Charge compensation is achieved with reduced oxygen, formally written as O^{2-}. The formal charge on the resultant diferric complex of EcBFR is zero[4] compared to −2 for the diferric complex of HuHF where the complex is hydrolyzed by 2 more equiv of base (*13*). However, at least one μ-oxo bridge appears to be a common feature of the ferroxidase center of both proteins as both show similar UV−visible difference spectra and molar absorptivities (Results, Figure 8) and Mössbauer spectra (*21*, *32*, *33*). The greater degree of hydrolysis of the HuHF complex and its negative charge probably account for its reduced stability and the tendency of the iron(III) in mammalian ferritin to translocate to nucleation sites and to the core where it becomes completely hydrolyzed according to eq 3, regenerating the ferroxidase site for processing more iron(II).

From the Zn^{2+} inhibition data, it is significant that phase 3 kinetics are not inhibited by the first 24 Zn^{2+} added to the protein; however, a decrease in rate with added Zn^{2+} is observed thereafter, reaching a minimum at 48 Zn^{2+} added (Figure 5). This observation can be explained by assuming that the first 24 Zn^{2+} bind cooperatively at 12 ferroxidase centers, thereby preventing formation of 12 ferric dimers. Provided that the 12 ferric dimers that are formed in the ferroxidase centers not containing Zn^{2+} are sufficient to support core formation at the normal rate, the 24 Zn^{2+} would not influence the phase 3 kinetics. When more than 24 Zn^{2+} are added, a correspondingly larger number of ferroxidase centers are blocked with a consequent decrease in the number of ferric dimers produced in the phase 2 reaction. When the number of ferric dimers drops below a certain level (between 7 and 12), they are insufficient to support core formation at the normal rate, and the phase 3 kinetics are affected.

Iron(II) oxidation is observed in the ferroxidase site variant E18A, although the rate is markedly slowed (Figure 6), an observation that reflects the kinetic advantage of an intact dinuclear ferroxidase center. The 24 Fe^{2+}/protein stoichiometry observed for the transition from the phase 2 to the phase 3 reaction of E18A (Figure 6, inset) suggests that the half of the dinuclear center remaining intact is capable of oxidizing iron, the net stoichiometries being $Fe^{2+}/O_2 = 4$ and $H^+/Fe = 2$. In this instance, the binding site may simply serve to facilitate iron(II) autoxidation as generally found for small Fe^{3+} chelates (*38*) and where complete reduction of O_2 to H_2O generally occurs. Further studies of this system are beyond the scope of the present work, however.

From the work presented here (and previous work), a model for iron uptake into bacterioferritin can be proposed. Each of the 24 ferroxidase centers binds 2 Fe^{2+} ions in a cooperative manner (eq 6, phase 1). In the presence of dioxygen, each dinuclear center undergoes oxidation, resulting in the formation of Fe^{3+} and H_2O (eq 7, phase 2). This reaction may proceed via a high-valent intermediate as described by eqs 10−13 or, alternatively, be a composite of two sequential reactions in which oxygen reacts at one center, yielding H_2O_2, which then reacts in preference to oxygen at another center, producing H_2O (eqs 14 and 15). The diferric form of the center is stable, with the two additional positive charges associated with the diferric center balanced by a μ-oxo bridge. Oxidation of iron(II) at the ferroxidase center is followed by nucleation and core formation (eq 9, phase 3). The diferric form of the center may serve as a catalytic center promoting nucleation and core formation through an outer sphere reaction. Alternatively, the diferric unit may undergo a rearrangement within the protein such that it continues to block the ferroxidase center (preventing regeneration) but also protrudes into the central cavity where it serves directly as a nucleation site for core formation. The data presented here do not address this latter question and, although previous data provide some evidence that a rearrangement occurs (*31*), this possibility requires further investigation.

Previous observation of mononuclear Fe^{3+} species during iron uptake by bacterioferritin resulted in the proposal that the diferric form of the center is unstable and breaks down immediately following oxidation (*24*). Quantitative EPR data reported here indicate that monomeric Fe^{3+} is *not* a major product following oxidation. Some monomeric Fe^{3+} (Figure 7, inset) is formed, however, and its role, if any, in the oxidation/mineralization mechanism of EcBFR is unclear. It may be a species formed in a minor pathway of iron accumulation in the protein or possibly represents nonspecifically bound Fe^{3+} or Fe^{3+} bound at nucleation sites since the EPR signal is attenuated upon further addition of iron. EPR signals at $g' = 4.3$ from mononuclear Fe^{3+} have been also observed in other ferritins (reviewed in refs *3* and *23*) and, based on Mössbauer data, have been attributed to breakup of the ferroxidase center dimer (*21*, *32*). However, a recent Mössbauer/EPR study suggests that the $g' = 4.3$ signal may arise from a trimeric Fe^{3+} species rather than monomeric Fe^{3+} (*39*).

In conclusion, the present work has revealed several new aspects of the mechanism of core formation in bacterioferritin. Despite the fact that bacterioferritins and mammalian ferritins utilize dinuclear ferroxidase sites to initiate iron core formation, they do so in quite different ways. Each type of ferritin is able to efficiently harvest iron from its environment and, through a specialized mechanism of oxidation and mineralization, store it in the form of a highly stable iron(III) oxide biomineral. The mechanism for EcBFR could have significance for the function that the protein fulfills in the cell. The complete reduction of dioxygen to water in EcBFR during iron oxidation may be important in the cell's response to oxidative stress. Further studies of other ferritins may well

[4] The formal charge of zero for the diferric complex of EcBFR comes from the sum of +6 (two Fe^{3+}), −4 (four glutamates), and −2 (O^{2-}, or two OH^-).

uncover additional mechanisms for core formation that have been adopted during the course of evolution. The newly discovered 12 subunit ferritin from *Listeria innocua* (*40*) may be a protein that possesses yet another core initiation and mineralizing mechanism.

ACKNOWLEDGMENT

We thank Dr. Simon Andrews for his gift of the EcBFR expression system, Mr. Junlong Shao for measuring the temperature dependence of the EPR spectrum, and Mr. John K. Grady for assistance with the spin concentration determinations.

REFERENCES

1. Chasteen, N. D., and Harrison, P. M. (1999) *J. Struct. Biol. 126*, 182.
2. Andrews, S. C. (1999) *Adv. Microb. Physiol. 40*, 281−351.
3. Chasteen, N. D. (1998) *Met. Ions Biol. Syst. 40*, 479−514.
4. Le Brun, N. E., Thomson, A. J., and Moore, G. R. (1997) *Struct. Bonding 88*, 104.
5. Harrison, P. M., and Arosio, P. (1996) *Biochim. Biophys. Acta Bio-Energetics 1275*, 161.
6. Levi, S., Yewdall, S. J., Harrison, P. M., Santambrogio, P., Cozzi, A., Rovida, E., Albertini, A., and Arosio, P. (1992) *Biochem. J. 288*, 591.
7. Levi, S., Santambrogio, P., Cozzi, A., Rovida, E., Corsi, B., Tamborini, E., Spada, S., Albertini, A., and Arosio, P. (1994) *J. Mol. Biol. 238*, 649.
8. Andrews, S. C., Smith, J. M. A., Yewdall, S. J., Guest, J. R., and Harrison, P. M. (1991) *FEBS Lett. 293*, 164.
9. Dautant, A., Meyer, J., Yariv, J., Precigoux, G., Sweet, R. M., Kalb, A. J., and Frolow, F. (1998) *Acta Crystallogr., Sect. D 54*, 16.
10. Andrews, S. C., Le Brun, N. E., Barynin, V., Thomson, A. J., Moore, G. R., Guest, J. R., and Harrison, P. M. (1995) *J. Biol. Chem. 270*, 23268.
11. Cheesman, M. R., Thomson, A. J., Greenwood, C., Moore, G. R., Andrews, and Kadire, F. H. A. (1990) *Nature 346*, 771.
12. Frolow, F., Kalb, A. J., and Yariv, J. (1993) *Acta Crystallogr., Sect. D 49*, 597.
13. Yang, X., Chen-Barrett, Y., Arosio, P., and Chasteen, N. D. (1998) *Biochemistry 37*, 9743.
14. Sun, S., and Chasteen, N. D. (1992) *J. Biol. Chem 267*, 25160.
15. Sun, S., Arosio, P., Levi, S., and Chasteen, N. D. (1993) *Biochemistry 32*, 9362.
16. Pereira, A. S., Small, W., Krebs, C., Tavares, P., Edmondson, D. E., Theil, E. C., and Huynh, B. H. (1998) *Biochemistry 37*, 9871.
17. Zhao, Z., Treffry, A., Quail, M. A., Guest, J. R., and Harrison, P. M. (1997) *J. Chem. Soc., Daltron Trans.*, 3977.
18. Andrews, S. C., Findlay, J. B. C., Guest, J. R., Harrison, P. M., Keen, J. N., and Smith, J. M. A. (1991) *Biochim. Biophys. Acta 1078*, 111.
19. Smith, P. K., Krohn, R. I., Hermanson, G. T., Mallia, A. K., Gartner, F. H., Provenzano, M. D., Fujimoto, E. K., Goeke, N. M., Olson, B. J., and Klenk, D. C. (1985) *Anal. Biochem. 150*, 76.
20. Falk, J. E. (1964) in *Porphyrins and Metalloporphyrins*, BBA Library, Vol. 2, p 181, Elsevier, North-Holland.
21. Bauminger, E. R., Harrison, P. M., Hechel, D., Nowik, I., and Treffry, A. (1991) *Biochim. Biophys. Acta 1118*, 48.
22. Yang, X., and Chasteen, N. D. (1996) *Biophys. J. 71*, 1587.
23. Sun, S., and Chasteen, N. D. (1994) *Biochemistry 33*, 15095
24. Le Brun, N. E., Wilson, M. T., Andrews, S. C., Guest, J. R., Harrison, P. M., Thomson, A. J., and Moore, G. R. (1993) *FEBS Lett. 333*, 197.
25. Le Brun, N. E., Keech, A. M., Mauk, M. R., Mauk, A. G., Andrews, S. C., Thomson, A. J., and Moore, G. R. (1996) *FEBS Lett. 397*, 159.
26. Keech, A. M., LeBrun, N. E., Wilson, M. T., Andrews, S. C., Moore, G. R., and Thomson, A. J. (1997) *J. Biol. Chem. 272*, 422.
27. Watt, G. D., Frankel, R. B., Jacobs, D., Huang, H., and Papaefthymiou, G. C. (1992) *Biochemistry 31*, 5672.
28. Xu, B., and Chasteen, N. D. (1991) *J. Biol. Chem. 266*, 19965.
29. Le Brun, N. E., Andrews, S. C., Guest, J. R., Harrison, P. M., Moore, G. R., and Thomson, A. J. (1995) *Biochem. J. 312*, 385.
30. Le Brun, N. E., Cheesman, M. R., Thomson, A. J., Moore, G. R., Andrews, S. C., Guest, J. R., and Harrison, P. M. (1993) *FEBS Lett. 323*, 261.
31. Le Brun, N. E., Andrews, S. C., Moore, G. R., and Thomson, A. J. (1997) *Biochem. J. 326*, 173.
32. Treffry, A., Bauminger, E. R., Hechel, D., Hodson, N. W., Nowik, I., Yewdall, S. J., and Harrison, P. M. (1993) *Biochem. J. 296*, 721.
33. Hawkins, C., Treffry, A., Mackey, J. B., Williams, J. M., Andrews, S. C., Guest, J. R., and Harrison, P. M. (1996) *Nuovo Cimento Soc. Ital. Fis., D 18*, 347.
34. Smith, R. M., and Martell, A. E. (1976) *Critical Stability Constants*, Vol. 4, pp 1 and 5, Plenum Press, New York.
35. Riggs-Gelasco, P. J., Shu, L.-J., Chen, S.-X. Burdi, D., Huynh, B. H., Que, L., and Stubbe, J. (1998) *J. Am. Chem. Soc. 120*, 849, and references cited therein.
36. Hsu, H.-F., Dong, Y., Shu, L., Young, V. G., Jr., and Que, L., Jr. (1999) *J. Am. Chem. Soc. 121*, 4230, and references cited therein.
37. Hwang, J., Krebs, C., Huynh, B. H., Edmondson, D. E., Theil, E. C., and Pennar-Hahn, J. E. (2000) *Science 287*, 122.
38. Harris, D. C., and Aisen, P. (1973) *Biochim. Biophys. Acta 329*, 156.
39. Pereira, A. S., Tavares, P., Lloyd, S. G., Danger, D., Edmondson, D. E., Theil, E. C., and Huynh, B. H. (1997) *Biochemistry 36*, 7917.
40. Bozzi, M., Mignogna, G., Stefanini, S., Barra, D., Longhi, G., Balenti, P., and Chiancone, E. (1997) *J. Biol. Chem. 272*, 3259.
41. Lawson, D. M., Artymiuk, P. J., Yewdall, S. J., Smith, J. M. A., Livingstone, J. C., Treffry, A., Luzzago, A., Levi, S., Arosio, P., Cesareni, G., Thomas, C. D., Shaw, W. V., and Harrison, P. M. (1991) *Nature 349*, 541.
42. Frolow, F., Kalb, A. J., and Yariv (1994) *Struct. Biol. 1*, 453.

BI992631F